Dendritic sidebranching with periodic localized perturbations: Directional solidification of pivalic acid–coumarin 152 mixtures

L. M. Williams, M. Muschol, X. Qian,* W. Losert, and H. Z. Cummins
Department of Physics, City College of New York, City University of New York, New York, New York 10031
(Received 8 February 1993)

We have studied the response of the sidebranches of pivalic acid dendrites, growing by directional solidification, to localized periodic thermal perturbations. The perturbations were generated by a laser beam focused near the tip of a single dendrite growing in a glass capillary, with the pulse duration, repetition rate, and intensity controlled separately. The perturbation dramatically altered the sidebranch structure, producing ordered sidebranches of well-defined wavelength, synchronous with the perturbation, which were strongly correlated on the two sides of the dendrite. The dependences of the sidebranch amplitude on the frequency of the perturbation and on the distance from the dendrite tip were compared to the predictions of Barber, Barbieri, and Langer [Phys. Rev. A **36**, 3340 (1987)] and found to be in qualitative agreement. The value of the selection parameter σ found from these fits to the theory is compared to a value, obtained from material parameters also determined in this experiment, and to a value deduced from the initial Mullins-Sekerka instability of the planar crystal-melt interface.

PACS number(s): 68.70.+w, 61.50.Cj, 81.30.Fb

I. INTRODUCTION

Considerable progress has been achieved during the past decade in understanding pattern-formation phenomena, since the introduction of the theoretical approach usually designated as "microscopic solvability" (for reviews, see [1–3]). One significant aspect of this field, which has received relatively little attention, is the sidebranching phenomenon which is an integral part of dendritic solidification. As noted recently by Langer [4], it is the evolution of dendritic sidebranches during the solidification of metallic alloys that ultimately determines the microstructure and resulting mechanical properties of the solid.

It is generally believed that sidebranches occur on growing dendrites as a result of selective amplification of microscopic noise present near the dendrite tip which is amplified as the perturbations travel down the sides of the dendrite, away from the tip. A theoretical description of this noise amplification mechanism, to be discussed below, was developed in a series of papers by Langer and his co-workers [5, 6].

Three previous experimental studies have provided evidence in support of this noise-amplification mechanism. Dougherty, Kaplan, and Gollub [7] studied the evolution of sidebranches on freely growing dendrites in supersaturated aqueous solutions of NH_4Br. They found that the power spectrum of the sidebranch oscillations at a fixed distance behind the tip is broad and noisy with little cross correlation between the two sides, consistent with theories in which sidebranching results from selective amplification of microscopic random noise. Dougherty and Gollub [8] also studied sidebranch spacing, demonstrating that the mean wavelength scales with the tip radius, as predicted by noise-amplification theories.

Qian and Cummins [9] investigated the response of a succinonitrile-acetone dendrite growing by directional solidification to a single brief localized laser-generated heat pulse applied near the dendrite tip. The resulting perturbation grew as it traveled down the dendrite, with a functional form in reasonable agreement with noise amplification models.

Bouissou *et al.* [10] studied the growth of dendrites solidifying from a flowing pivalic acid– (PVA) ethanol solution when the solution flow velocity was periodically modulated. This global periodic perturbation was found to induce ordered dendritic sidebranches coherent with the flow modulation. The amplitude dependence of the response function was investigated and was found to be linear over a considerable range. The frequency dependence was shown to exhibit a maximum, indicating that the noise amplification mechanism is selective. A related experiment was reported by Rabaud, Couder, and Gerard *et al.* [11] in which anomalous Saffman-Taylor fingers, subjected to periodic modulation of the forcing pressure, exhibited a sidebranching wave whose amplitude also depended on the forcing frequency.

We have carried out an experimental study of dendritic sidebranching in pivalic acid containing coumarin 152 as the solute, in which a focused laser beam produced a periodic localized thermal perturbation near the tip of a dendrite growing by directional solidification. This perturbation dramatically alters the sidebranch structure of the dendrite. The perturbed dendrite exhibits highly ordered sidebranches, coherent on either side of the dendrite, that appear closer to the tip than the natural sidebranches. These induced sidebranches are synchronous with the perturbation, in agreement with the noise-amplification theory of sidebranching [5] and the experimental results of Bouissou *et al.* [10].

We have studied the variation of the amplitude of the perturbation-induced sidebranches as a function of the frequency of the perturbation and obtained a response curve which we will compare with the predictions of Barber, Barbieri, and Langer [6]. The results will also be compared with those of Bouissou *et al.* [10]. Furthermore, we have studied the variation of the response curve with growth velocity, distance down the dendrite, and temperature gradient. We have also studied the increase in sidebranch amplitude with distance from the dendrite tip, and compared this result with the predictions of Barber, Barbieri, and Langer [6]. In fitting our data, the selection parameter σ of microscopic solvability theory was treated as a free parameter that was varied to fit the data. We compare the values of σ obtained from these fits with a direct determination of σ^c, calculated using experimental measurements of the capillary length d_0^c, the chemical diffusion constant D^c, the tip velocity v, and the tip radius ρ ($\sigma^c = 2d_0^c D^c/\rho^2 v$), as well as with a preliminary value of σ obtained from an observation of the initial Mullins-Sekerka instability of the planar crystal-melt interface.

II. EXPERIMENT

A. Sample preparation and apparatus

Samples were prepared from PVA, purchased from Aldrich, which was triply distilled and then doped with 0.44 wt. % of coumarin 152 (C152, a yellow laser dye purchased from Sigma Chemical Co., St. Louis) as the solute. C152 was chosen as the solute in order to enhance the absorption of the laser light to a level necessary to create a significant thermal perturbation. Its fluorescence also provides a convenient means of determining the solute concentration field.

The samples were loaded into 20 cm×50 μm×1 mm rectangular glass capillaries (Vitro Dynamics) and sealed with epoxy. The sample capillary was attached to a Velmex Unislide precision motor-driven stage equipped with a dc motor that can pull the capillary at a constant speed in the range 0–40 μm/s. Our directional solidification apparatus consists of a brass housing equipped with sapphire windows. The capillary is translated longitudinally within a paraffin-oil-filled channel inside the housing, located between two temperature-controlled copper heating or cooling blocks that provide the temperature gradient. The hot block is elongated to keep the entire liquid side of the sample molten. This directional solidification apparatus is mounted on the stage of a Nikon Diaphot inverted microscope equipped with a video camera (MTI-Dage series 68 Nuvicon). We use a 10× long-working-distance objective and a 1× projection lens in the video port. The video camera is interfaced to a digital image processing board (Data Translation "Quick capture") in a Macintosh II ci computer and provides images consisting of 640 × 480 pixels at 30 frames/s. One pixel corresponds to an area of approximately 2 μm × 2 μm in the sample.

B. Experimental procedure

Dendrites were typically grown in a temperature gradient G of about 25 K/cm at a velocity in the range of 2–4 μm/s, which produced dendrites of tip radii $\rho \sim$10–15 μm. To provide the perturbation, short pulses of laser light were focused in the melt close to the tip of the growing dendrite. The light source was a Spectra Physics 165 argon-ion laser operating at 457.9 nm. The laser output beam, after traversing an electronic shutter, was transmitted through a 7-μm inner-core-diameter optical fiber to a focusing lens mounted on the microscope stage. This lens produces a spot approximately 6 μm in diameter in the sample. In a typical experiment the laser beam was chopped to produce a periodic train of pulses of width 1.0 s, with period τ_r between 10 and 60 s.

At the beginning of an experiment a single dendrite is grown out of a precisely oriented seed crystal. After an initial transient stage the dendrite reaches a steady state and attains a growth speed equal to the capillary pulling speed. At steady state, the tip of the dendrite is stationary in the laboratory frame, with sidebranches propagating down both sides of the dendrite.

The laser spot is positioned in the melt about one tip radius ahead of the tip, and the periodic perturbation is turned on. Initially the tip moves back slightly, and the position of the laser spot is then readjusted. Once the perturbed tip reaches a new steady state, the position of the laser spot is kept constant, and data are accumulated. For each period of the pulse train, corresponding to one point on the response curve, data are recorded for typically ten minutes.

During a run it is important that the distance between the tip and the perturbation remains reasonably constant. Several precautions were taken to maintain this constant distance. The seed must be precisely oriented (ours are oriented to better than 0.1°), otherwise the tip will move to the side of the capillary during the run. The dendrite must also grow into a melt that has a uniform impurity concentration. To ensure that this was the case, once our samples had a suitable seed they were left in the apparatus for several days with the entire liquid side of the capillary molten; this allows the dye distribution to equilibrate.

III. THEORY

During the past decade, it was discovered that the equations governing solidification of low-anisotropy crystals, with the surface tension properly included from the outset, led to a denumerably infinite set of solutions of which only one is stable [12, 2]. This "microscopic solvability" result showed that the surface tension and its (small) anisotropy play a crucial role in determining the tip radius and growth velocity of a dendrite. However, the smooth nearly parabolic needle crystals predicted as stable solutions are not observed in real dendrites which exhibit sidebranching.

Pieters and Langer first suggested that sidebranches might be generated by selective amplification of noise near the locally stable tip [5, 2]. They analyzed this mech-

anism for the two-dimensional boundary layer model, following a method previously employed by Zel'dovich *et al.* [13] for flame fronts, which showed that, although perturbations would die out locally, they could be amplified as they traveled down the sides of the dendrite. The calculation was extended to three dimensions by Langer [14]. Kessler and Levine [15] studied the symmetric model numerically and predicted that the wavelength of sidebranches generated by noise amplification should scale with tip radius, a prediction subsequently verified by Dougherty and Gollub [8].

Barber, Barbieri, and Langer [6] performed an analytic study of sidebranching in the two-dimensional symmetric model using the WKB method. They found that in the presence of a sinusoidal perturbation the response function, defined as the sidebranching amplitude divided by the amplitude of the perturbation, would be given by

$$W(x,\omega) \propto e^{i\omega(t-x^2/2)/\sqrt{\sigma}} e^{\omega[x-\omega^2 B(x)]/\sqrt{\sigma}} \tag{3.1}$$

where $B(x)$ is

$$B(x) = 8x(1+x^2)^{1/2} + \frac{8x}{(1+x^2)^{1/2}} - 15s(x)$$

with

$$s(x) = \frac{1}{2}\ln[x+(1+x^2)^{1/2}] + \frac{1}{2}x(1+x^2)^{1/2} .$$

In Eq. (3.1) [Eq. (3.28) in Ref. [6]], the length unit is ρ, the time unit is ρ/v, and the unit of ω is $v/(\rho\sqrt{\sigma})$. We also define the dimensionless period $\bar{\tau} = \tau v/\rho$. The dimensionless parameter σ is given by

$$\sigma = 2d_0 D/\rho^2 v \tag{3.2}$$

where d_0 is the thermal capillary length, $d_0 = \gamma T_m c/L^2$ (γ is the surface tension, T_m is the melting temperature, c is the specific heat, and L is the latent heat), and D is the thermal diffusion coefficient. In these units, the parabolic approximation for the shape of the dendrite is $z = -x^2/2$. Therefore, x is the half-width of the dendrite at the location of the scan line, which cuts the dendrite axis at a distance z from the tip.

As $x \to +\infty$, $B(x) \to \frac{1}{2}x^2 + O(\ln x)$ and the response function becomes

$$W(x,\omega) \propto e^{i\omega(t-x^2/2)/\sqrt{\sigma}} e^{\omega[x-\omega^2 x^2/2]/\sqrt{\sigma}} . \tag{3.3}$$

In Fig. 1(a) we plot $B(x)$ along with its asymptotic approximation $x^2/2$. For our purposes it is more convenient to fit our data to $W(\bar{\tau},x)$. In Fig. 1(b) we plot $W(\bar{\tau},x)$ (at $\sigma = 0.05$) as a function of $\bar{\tau}$ for several values of x. For larger values of x, $W(\bar{\tau},x)$ is qualitatively similar to what we see in our experiments. However, for lower values of x, $W(\bar{\tau},x)$ diverges as $\bar{\tau} \to 0$, and thus no longer resembles our data, which always exhibit a maximum. This behavior occurs when the function $B(x)$ becomes negative, thus causing the exponent in Eq. (3.1) to be positive for all values of ω, so the $W(\omega,x)$ has no maximum. As our data are taken at values of x close to the region in which Eq. (3.1) no longer qualitatively describes the observed growth of the sidebranches we have fitted

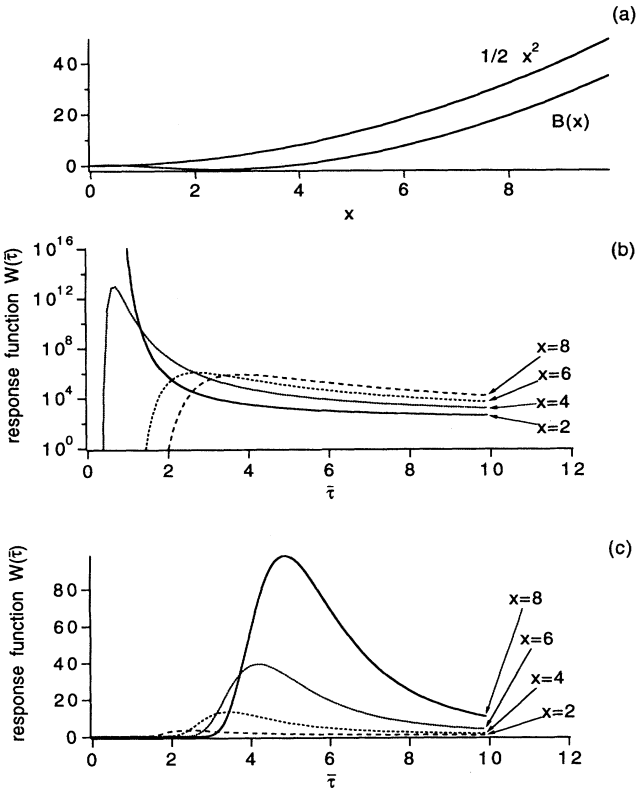

FIG. 1. (a) $B(x)$ vs x, and its asymptotic form as $x \to \infty$, $B(x) = x^2/2$. (b) $W(\bar{\tau})$ vs $\bar{\tau}$ for several values of x using the full form of $B(x)$. (c) $W(\bar{\tau})$ vs $\bar{\tau}$ for several values of x using $B(x) = x^2/2$.

our data to Eq. (3.3). In Fig. 1(c) we plot the asymptotic form $W(\bar{\tau},x)$ [i.e., taking $B(x) = x^2/2$] as a function of $\bar{\tau}$ for several values of x. This form of $W(\bar{\tau},x)$ now qualitatively has the appropriate behavior for low values of $\bar{\tau}$ and x. The choice of using Eq. (3.3) rather than Eq. (3.1) to fit our data was reinforced after preliminary attempts to fit data to Eq. (3.1) gave unphysical values of σ. (For a discussion of σ see Sec. V.)

The shape of the response curve predicted by Eq. (3.3) is determined by the factor $e^{\omega(x-\omega^2x^2/2)/\sqrt{\sigma}}$, which predicts that for a given x, $W(\bar{\tau})$ should have a maximum at $\bar{\tau}_p = \sqrt{6\pi^2\sigma x}$.

The theoretical analyses discussed in this section were carried out for free solidification of pure materials. We are not aware of any theoretical studies of sidebranch amplification during directional solidification of binary alloys. Therefore, we will attempt to fit our data to Eq. (3.3), treating both the scale factors and the selection parameter σ as adjustable fitting parameters.

IV. RESULTS AND ANALYSIS

A. Qualitative effect of the perturbation

Unperturbed dendrites in our experiment displayed sidebranching characteristics similar to those reported by

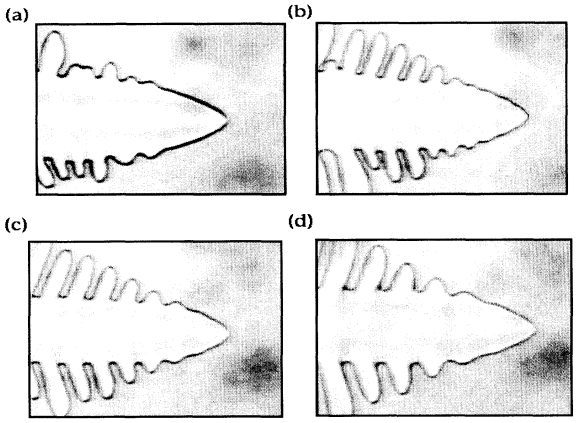

FIG. 2. Video images of dendrites grown by directional solidification from a mixture of pivalic acid and 0.44 wt.% coumarin 152. v=3.7 μm/s. (a) No perturbation; (b) 1-s laser pulses with a repetition rate of $\tau_r = 15$ s; (c) repetition rate of $\tau_r = 19$ s, which is close to the natural period; (d) repetition rate of $\tau_r = 26$ s.

Dougherty, Kaplan, and Gollub [7], and by Bouissou *et al.* [10]. The spontaneous sidebranches were irregular and only approximately periodic, and there was little correlation between the sidebranches on the two sides of the dendrite [see Fig. 2(a)]. When the periodic perturbation was applied, the sidebranches became visible closer to the tip. These induced sidebranches, generated by the laser perturbation, then propagated down the sides of the dendrite. The previously irregular sidebranch structure was transformed into a regular periodic structure with a well-defined wavelength, and the patterns on the two sides of the dendrite became highly correlated. This ordered region eventually extended down the dendrite over a region of typically six to twelve sidebranches. There was then a transient period during which the amplitude of the sidebranches in the ordered region grew, after which the sidebranch pattern appeared to be stable. Once this stable pattern was established, data were recorded. If the perturbation was interrupted, even if only missing a single pulse, the subsequent sidebranch structure was diminished and only regained its previous amplitude after several cycles of the perturbation. Typical images of a stable perturbed dendrite are shown in Figs. 2(b)–2(d).

B. Analysis

To extract the tip radius ρ, a parabola was fitted through the tip region of the dendrite. The fitting range of the parabola was restricted to a region of 4ρ from the tip. (This procedure is similar to that reported by Dougherty and Gollub [8].)

For precision studies of the sidebranching dynamics, a single video line was recorded repeatedly at four times per second. Typically, the scan line was chosen to cut across the dendrite perpendicular to the growth direction ~15 tip radii back from the tip. The time-dependent positions of the two edges of the dendrite were extracted from the intensity profile along each video line by parabolic interpolation. (For a description of this interpolation procedure, see Ref. [16].) A typical time record of the position of one edge versus time for an unperturbed dendrite is shown in Fig. 3(a); its Fourier transform is shown in Fig. 3(b). The spectra of both edges exhibit noisy broadband spectra, peaking near 0.055 Hz, indicating a "natural" sidebranching period of $\tau_n \sim 18$ s.

In Fig. 4(a), a record of edge position versus time is shown for a dendrite perturbed with pulses at a fundamental period of $\tau_r = 19$ s which is close to the natural period of the unperturbed dendrite. The corresponding Fourier spectrum in Fig. 4(b) shows a sharp peak that is synchronous with the perturbation. Again it is apparent that the periodic perturbation dramatically alters the sidebranching process, converting a noisy broadband structure into a nearly monochromatic narrow-band sidebranch spectrum.

C. The response function

To determine how the response of the dendrite varies with the period of the perturbation, 12 runs of about 8–15 min were recorded, the length of the run being set to record the passage of about 40 sidebranches. In each run the dendrite was perturbed at a different period that varied from about 3/4 of the natural period to about twice the natural period.

From the Fourier transform of the time record of the

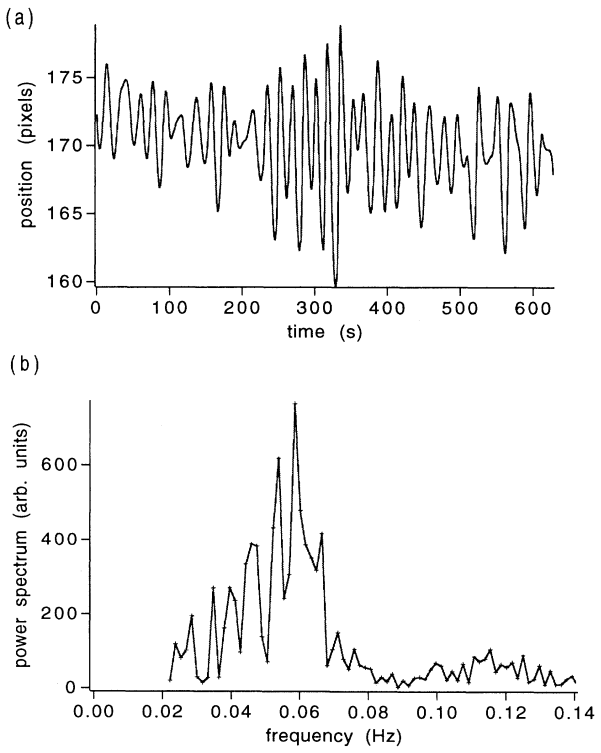

FIG. 3. (a) Record of the position of one edge of the unperturbed dendrite vs time. $v = 2.9$ μm/s. (Units of position in pixels; 1 pixel = 2.0 μm.) (b) Fourier transform of (a).

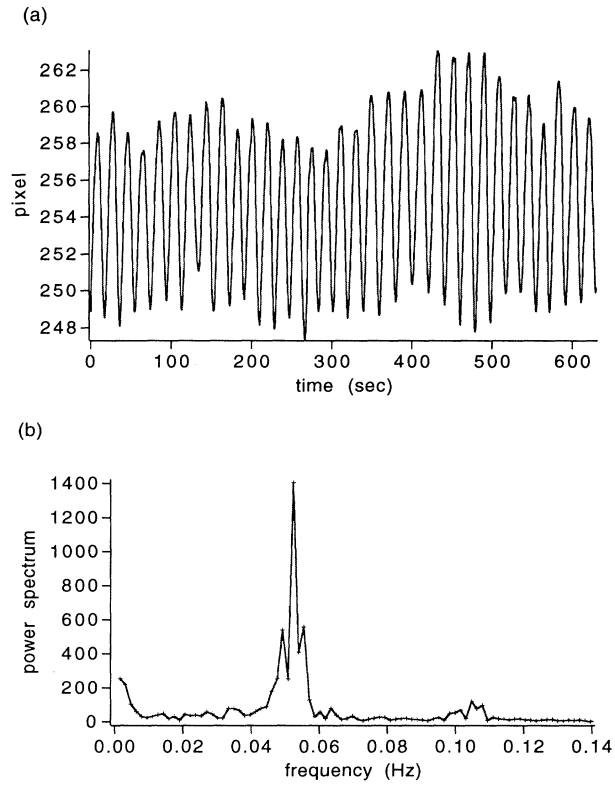

FIG. 4. (a) Time record of the position of one edge of the dendrite vs time for a perturbed dendrite. $v = 2.9$ μm/s. The fundamental period of the perturbation is 19 s, which is close to the natural period. (Units of position in pixels; 1 pixel = 2.0 μm.) (b) Fourier transform of (a).

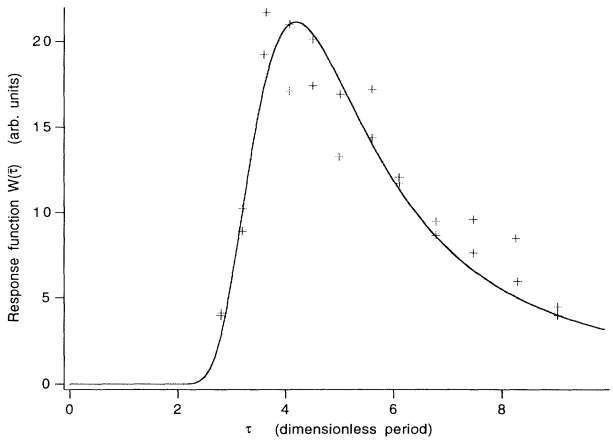

FIG. 5. Sidebranching response function W of a perturbed dendrite plotted against the dimensionless period $\bar{\tau} = \tau v/\rho$. $v = 2.9$ μm/s, tip radius $\rho = 13.7$ μm, gradient $G = 26$ K/cm. The solid line is a two-parameter fit to $W = Ae^{\omega(x-\omega^2 x^2/2)/\sqrt{\sigma}}$ where $x = 4.7$ is the width of a parabolic approximation to the dendrite. The fit gave $A = 192 \pm 10$ and $\sigma = 0.0630 \pm 0.0015$. The peak of the fitted response curve is at $\bar{\tau}_p = 4.19 \pm 0.05$.

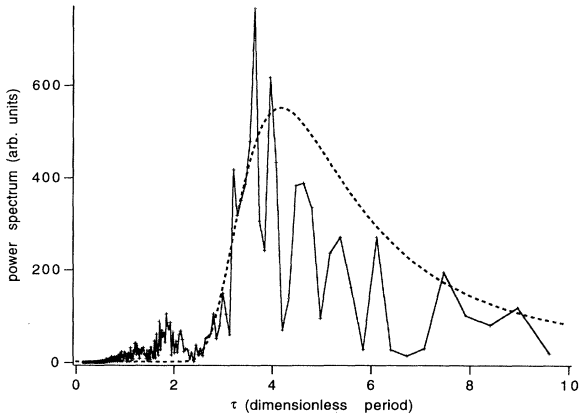

FIG. 6. Sidebranch spectrum of the unperturbed dendrite shown in Fig. 3(b), replotted with the frequency scale expressed in units of the dimensionless period. The dashed line is the response curve of Fig. 5 rescaled to approximately the same amplitude as the unperturbed sidebranch spectrum.

edge position for each perturbation period τ_r we determined the response function $W(\bar{\tau})$ of the dendrite, defined as the ratio of the amplitude of the fundamental Fourier component of the sidebranches to the fundamental Fourier component of the perturbation, as shown in Fig. 5. (In this experiment, $v = 2.9$ μm/s and $\rho = 13.7$ μm, so that the unit of time is 4.69 s.) The response function $W(\bar{\tau})$ has a maximum near 4.2 corresponding to the natural period of $\tau_0 \sim 20$ s.

We fit the prediction of Barbieri *et al.* [Eq. (3.3)] to our experimental data, treating both the scale factor and σ as free parameters. The fit indicated by the solid line in Fig. 4 was obtained with $\sigma = 0.0630 \pm 0.0015$. The maximum of the fitted curve is at $\bar{\tau}_p = 2\pi\sqrt{\sigma}/\omega_p = 4.18$.

If we replot the unperturbed spectrum of Fig. 3 (b) in the same units as in Fig. 5 (see Fig. 6) we notice that $W(\bar{\tau})$ is also qualitatively similar to the envelope of the unperturbed spectrum. This is a good indication that the sidebranch spectrum of an unperturbed dendrite results from the intrinsic sidebranching response excited by spontaneous white noise.

D. Variation of the response curve with position of the scan line, growth velocity, and temperature gradient

As noted by Barber *et al.*, Eq. (3.3) peaks at $\bar{\tau}_p^2 \approx 6\pi^2 x\sigma$, so that the response function should peak at longer periods as one moves down the dendrite. In order to investigate this prediction, we determined additional response curves at $x = 4.0$ and 5.6. The locations on the dendrite of these scan lines (and of the x=4.7 scan line discussed in the previous section) are illustrated in Fig. 7. One is limited to a relatively small range in x over which reliable data can be obtained. At larger values of x the sidebranches bend over and a given scan line will pass through more than one sidebranch on either side of

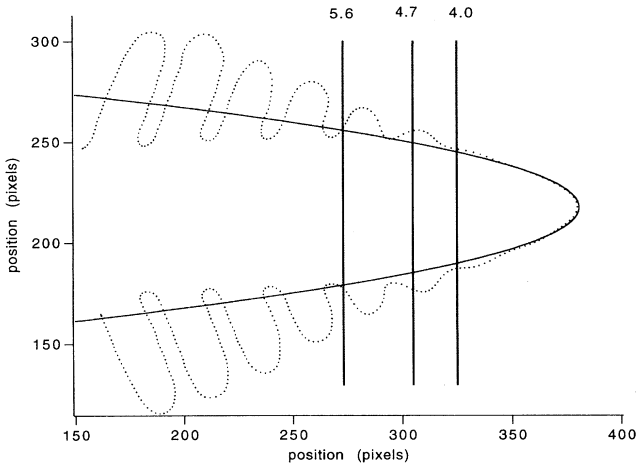

FIG. 7. Perturbed interface profile (dots) for a perturbation with period τ_r=19 s, close to the natural sidebranching period. v = 2.9 μm/s, tip radius ρ = 13.7 μm, gradient G = 26 K/cm. Vertical lines indicate positions of cuts for data taken at x=4.0, 4.7, and 5.6.

the dendrite; for smaller values of x the sidebranches are too small to be well resolved, especially for perturbing periods far from the peak of the response curve.

In Fig. 8 we show the response curves for x=4.0 and 5.6. In Fig. 9 the values of σ extracted from the three fits are plotted against z, the distance along the dendrite's axis from the tip, in units of the tip radius. In Fig. 10, we plot $\bar{\tau}_p$ against z. The corresponding period in seconds is indicated on the right-hand axis. The resulting variation in τ_p indicates that there is little change in wavelength as the train of sidebranches propagates down the dendrite, at least in the range where the perturbation has ordered the sidebranches. This result suggests that once the sidebranches become large enough to be out of the linear regime, their wavelength becomes locked in by nonlinearities not taken into account in the theory. We will return to this point in Sec. VI.

We next investigated the variation of the response curve with growth velocity. In Fig. 11 we plot response curves for v = 2.2 μm/s and 3.9 μm/s (both taken at x = 4.7). Again, the range over which it is possible to record reliable data is limited by experimental considerations. It was not possible to collect data at higher velocities since additional dendrites would start to grow alongside the perturbed dendrite, while at slower velocities the distance between the dendrite tip and the laser spot is more prone to drift.

In Fig. 12 we plot the σ values found from the above fits versus the growth velocity v for the three runs. An unexpected decrease in σ with increasing v is seen. In Fig. 13 we plot the position of the peak of the response curve ($\bar{\tau}_p$) against v. The corresponding period in seconds is indicated on the right-hand axis. If one interprets the position of the peak of the response curve as the "natural" period or wavelength of an unperturbed dendrite, one can see that for a large change in the natural period τ_p, from $\sim$ 14 to $\sim$ 30 s, the change in the dimension-

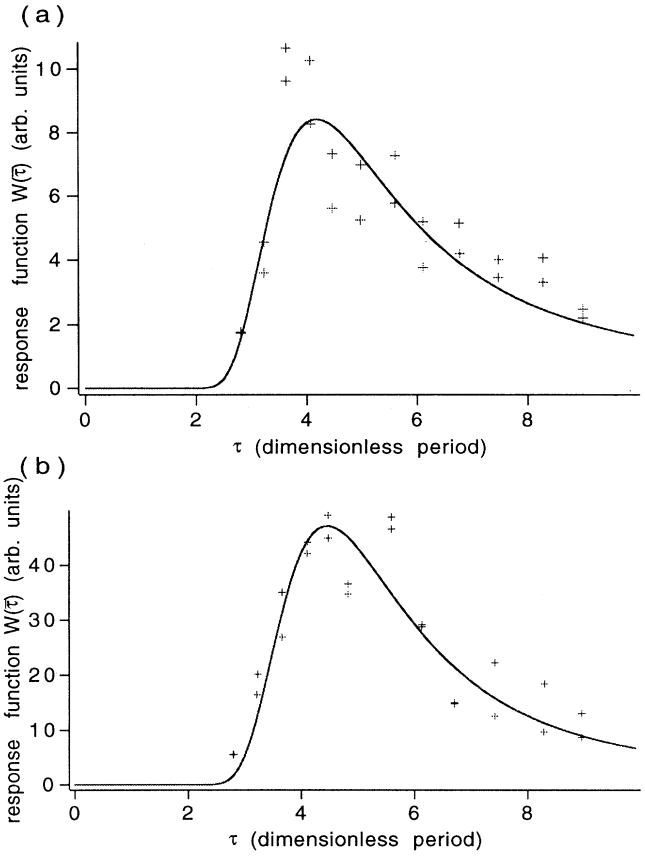

FIG. 8. Sidebranching response function W of a perturbed dendrite plotted against the dimensionless period $\bar{\tau} = \tau v/\rho$. The solid lines are two-parameter fits to $W = Ae^{\omega(x-\omega^2x^2/2)/\sqrt{\sigma}}$ where x is the width of a parabolic approximation to the dendrite. v = 2.9 μm/s, tip radius ρ = 13.7 μm, gradient G = 26 K/cm. (a) The cut is taken at x = 4.0. Fit result: $A = 153 \pm 12$ and $\sigma = 0.0738 \pm 0.0027$. The peak of the fitted response curve is at $\bar{\tau}_p = 4.18 \pm 0.08$. (b) The cut is taken at x=5.6. Fit result: $A = 218 \pm 17$ and $\sigma = 0.0575 \pm 0.0016$. The peak of the fitted response curve is at $\bar{\tau}_p = 4.36 \pm 0.06$.

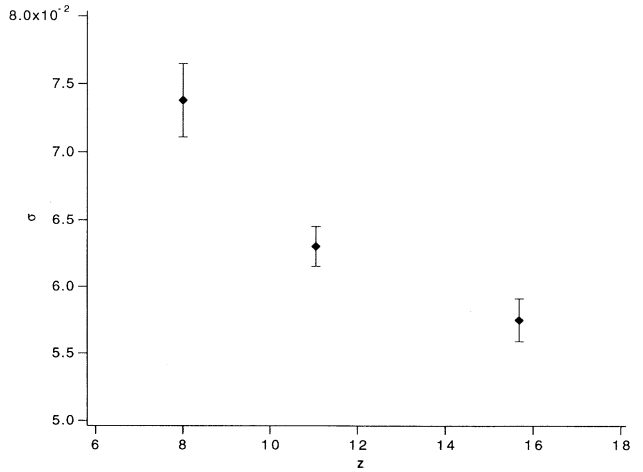

FIG. 9. Values of σ from fits to Eq. (3.3) vs distance from the dendrite tip (z), in units of tip radius.

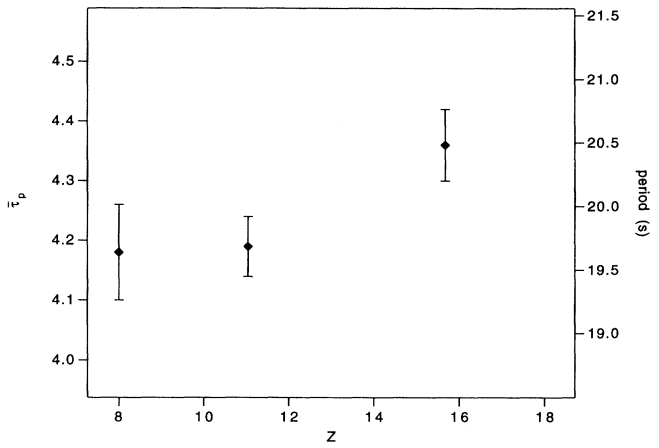

FIG. 10. Position of the peak of fitted response curve, $\bar{\tau}_p = \tau_p v/\rho$, vs distance from the tip, in units of tip radius. The corresponding period (in seconds) is indicated on the right-hand axis.

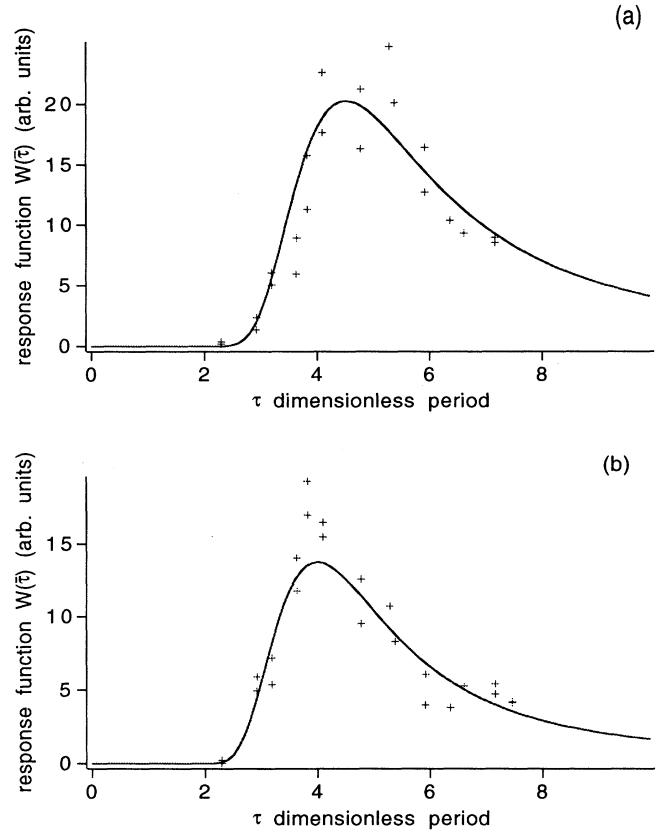

FIG. 11. Sidebranching response W of perturbed dendrite vs the dimensionless period $\bar{\tau} = \tau v/\rho$. The solid lines are two-parameter fits to $W = Ae^{\omega(x-\omega^2x^2/2)/\sqrt{\sigma}}$ where x is the width of a parabolic approximation to the dendrite. The cut is taken at x=4.7. (a) v = 2.2 μm/s, tip radius ρ = 15.0 μm, gradient G=26 K/cm. Fit result: $A = 258 \pm 15$ and $\sigma = 0.0731 \pm 0.0014$. The peak of the fitted response curve is at $\tau_p = 4.51 \pm 0.04$. (b) v=3.9 mm/s, tip radius ρ = 12.9 μm, gradient G=26 K/cm. Fit result: $A = 99 \pm 8$ and $\sigma = 0.0572 \pm 0.0015$. The peak of the fitted response curve is at $\tau_p = 3.99 \pm 0.05$.

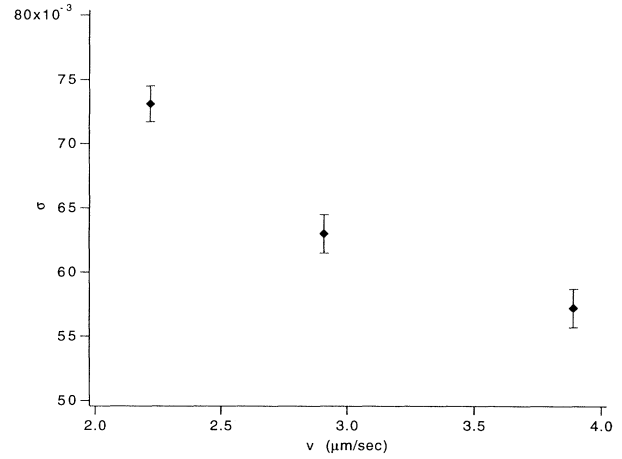

FIG. 12. Values of σ vs growth velocity v of the dendrite extracted from fits to Eq. (3.3).

less $\bar{\tau}_p$ is relatively small, i.e., one can almost double the growth velocity and the wavelength of the sidebranches remains approximately four times the tip radius, consistent with the prediction that the wavelength of the sidebranches scales with the tip radius. (This result agrees with the observation of Dougherty and Gollub [8].)

Finally, we determined a response curve at a different temperature gradient. In Fig. 14 we plot the response curve for G = 32 K/cm (with v = 2.9 μm/s and x=4.7). The fit to Eq. (3.3) gives $\sigma = 0.078 \pm 0.003$ and $\bar{\tau}_p = 4.36 \pm 0.06$. If this is compared to the response curve taken at the same velocity and x but with G=26 K/cm, we see there is quite a significant shift in $\bar{\tau}_p$. This suggests that the dimensionless $\bar{\tau}_p$ may be sensitive to changes in the temperature gradient. Further studies are in process to investigate this dependence and will be reported in a later publication.

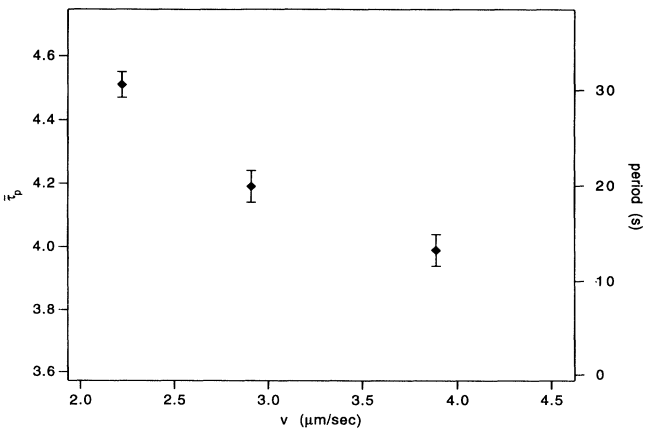

FIG. 13. Position of the peak of fitted response curve, $\bar{\tau}_p = \tau_p v/\rho$, vs growth velocity of the dendrite. The corresponding period (in seconds) is indicated on the right-hand axis.

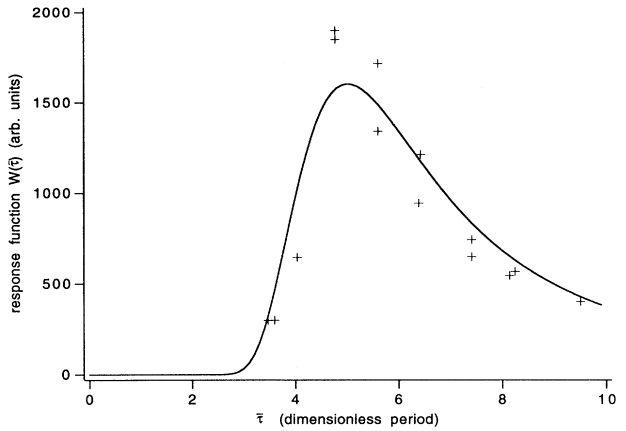

FIG. 14. Sidebranching response function W of perturbed dendrite plotted against the dimensionless period $\bar{\tau} = \tau v/\rho$. The solid line is a two-parameter fit to $W = Ae^{\omega(x-\omega^2 x^2/2)/\sqrt{\sigma}}$ where x is the width of the parabolic approximation to the dendrite. The cut is taken at $x = 5.6$. $v = 2.9$ μm/s, the tip radius $\rho = 13.7$ μm, gradient $G = 32$ K/cm. Fit result: $A = 218 \pm 17$ and $\sigma = 0.0575 \pm 0.0016$. The peak of the fitted response curve is at $\bar{\tau}_p = 4.36 \pm 0.06$.

E. Growth of the sidebranch amplitude with distance

We have also tested the prediction of Barber, Barbieri, and Langer [6] for the growth of sidebranches with distance from the dendrite tip. A series of 15-min scans similar to the one shown in Fig. 4(a) were recorded at 13 locations along the dendrite with the period of the perturbation close to the peak of the response curve. For each scan, the average positions of the peaks and troughs of the sidebranches was calculated, and the sidebranch amplitude was taken to be the difference between these two values. The perturbing period was $\tau = 19$ s ($\bar{\tau} = 4.04$). At this value of $\bar{\tau}$ both the full and asymptotic forms of $W(\bar{\tau})$ can reasonably describe the sidebranching [from Fig. 1(b) we can see that the region of unphysical behavior of $W(\bar{\tau})$ occurs at lower values of $\bar{\tau}$]. In Fig. 15 we plot the sidebranch amplitude against x. We have fitted the data with both the full and asymptotic form of the response function. The values of σ extracted from the fit were $\sigma = 0.046 \pm 0.002$ and 0.037 ± 0.002 for the full and asymptotic forms, respectively, for the lower edge of the dendrite, and $\sigma = 0.051 \pm 0.002$ and 0.04 ± 0.002 for the upper edge. One can see that both forms provide a reasonable fit, with the full function being slightly better.

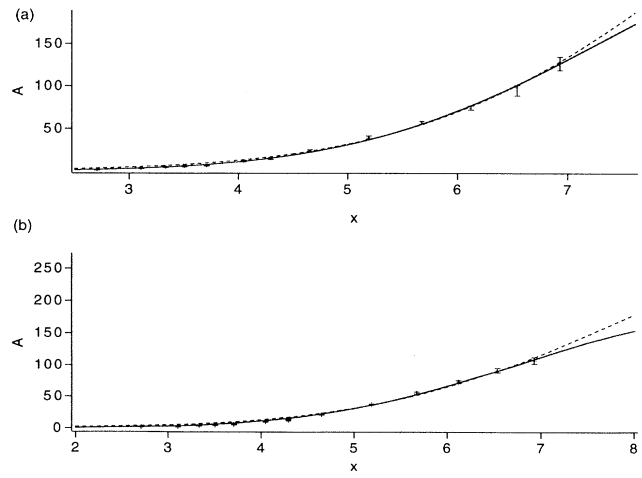

FIG. 15. Sidebranch amplitude vs x. Solid line represents a fit to $W(x)$ of Eq. (3.1) with the full form of $B(x)$; dashed line represents a fit to the asymptotic form of $W(x)$. (a) Upper edge: fit to full $W(x)$ gives $\sigma = 0.051 \pm 0.002$, fit to asymptotic $W(x)$ gives $\sigma = 0.040 \pm 0.002$. (b) Lower edge: fit to full $W(x)$ gives $\sigma = 0.046 \pm 0.002$, fit to asypmtotic $W(x)$ gives $\sigma = 0.037 \pm 0.002$.

V. MATERIAL CHARACTERIZATION AND DETERMINATION OF σ

A. Material characterization

In theoretical models of the morphology of solidifying binary systems, the length scale of the microstructure arises from two competing mechanisms. The destabilizing effect of impurity diffusion is characterized by the diffusion length $l^c = 2D^c/v$, where D^c is the chemical diffusion constant of the solute in the melt, and v is the growth velocity of the dendrite. The stabilizing effect of the surface tension is characterized by the capillary length d_0^c. For growth from a dilute solution, d_0^c is given by [17]

$$d_0^c = \frac{\gamma}{L} \frac{T_m}{(T_m - T_i)(1-k)} \ . \tag{5.1}$$

To calculate d_0^c, values for the surface tension $\gamma = 2.84 \times 10^{-7}$ J/cm^2, and the latent heat $L = 2267.7$ J/mole, were taken from the literature [18]. Values for the segregation coefficient k, the interface temperature T_i, and the melting temperature of the pure material T_m, as well as D^c and v, were experimentally determined.

(1) The segregation coefficient k. To determine the segregation coefficient a sample was mounted in the directional solidification apparatus and grown for a short time at a low pulling speed to establish a region of the crystal having a uniform dye concentration. The growth time and pulling speed were chosen so that the solute concentration ahead of the advancing solidification front did not build up significantly before growth was stopped. The sample was then allowed to equilibrate for several days. The laser beam (at low intensity to avoid melting the crystal) was focused to a spot inside of the sample. A second optical fiber picked up the fluorescent light which after passing through suitable filters was measured by a photomultiplier.

The sample stage was moved back and forth to position either the solid or the liquid side of the interface at the laser spot, and the fluorescent intensity was measured by accumulating photocounts for typically 60 s. After subtraction of the background intensity, the segregation

coefficient was taken as $k = I_{\text{solid}}/I_{\text{liquid}}$. (We verified that I is proportional to C for concentrations C up to ~ 1 wt.%, and that the fluorescent efficiency is the same for the solid and the liquid.) For 0.44 wt.% PVA-C152, this procedure gave $k = 0.06 \pm 0.01$.

(2) The chemical diffusion constant D^c. Following the same initial procedure as in (1), the solid-liquid interface was equilibrated, the laser beam was positioned on the solid side of the interface, and the fluorescence intensity was recorded. The hot block temperature was suddenly increased, causing the solid-liquid interface to melt back rapidly. The concentration step which existed in equilibrium at the solid-liquid interface was then located in the melt and began to decay immediately as dye diffused into the low concentration region previously occupied by the crystal.

We monitored the increase of concentration with time by following the fluorescence intensity $C(z,t)$ at fixed position z. $C(z,t)$ is predicted by the standard solution to the diffusion equation for an initial concentration step at $z = 0$ to be

$$C(z,t) = C_s + (1/2)(C_l - C_s)\text{erfc}(z/\sqrt{4D^c t}) \quad (5.2)$$

where C_l and C_s are the initial dye concentrations in the liquid and solid, respectively, and erfc is the complementary error function. The fluorescent intensity record was fit to Eq. (5.2) (with z and D^c as fitting parameters) to determine D^c (see Fig. 16). For our sample, the average result of two measurements was $D^c = 9.1 \pm 0.2 \times 10^{-7}$ cm^2/s.

(3) The interface temperature T_i. The temperature of the interface was determined by recording the position of the tip of the dendrite and then measuring the temperature profile in the cell. This procedure gave $T_i = 33.9 \pm 0.1\,^\circ$C, We determined the melting temperature of the pure material to be $35.9 \pm 0.1\,^\circ$C. Thus our interface was $2.0 \pm 0.1\,^\circ$C below T_m.

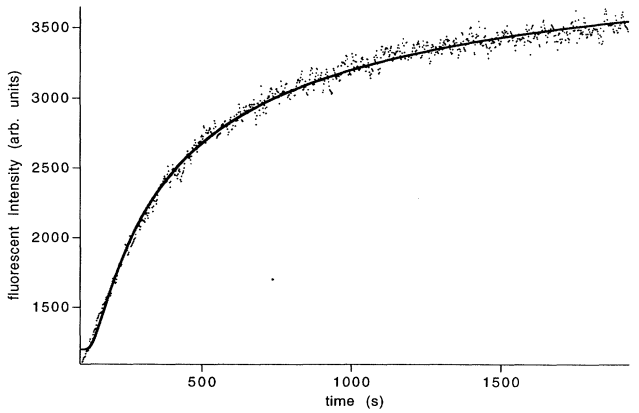

FIG. 16. Determination of the chemical diffusion constant D^c from the fluorescent intensity vs time, after the interface was melted back. The data were fit to $C(z,t) = C_s + (1/2)(C_l - C_s)\text{erfc}(z/\sqrt{4D^c t})$ as discussed in the text. For this measurement the result of the fit was $D^c = 8.9 \times 10^{-7}$ cm^2/s.

TABLE I. Values of physical constants for the PVA-C152 mixture (values refer to PVA except where noted otherwise).

Parameter	Value	Ref.
$MW_{PVA}(g)$	102.13	[18]
$MW_{C152}(g)$	257.2	a
γ (J/cm^2)	2.84×10^{-7}	[18]
L (J/mole)	2267.7	[18]
T_m (K)	35.970	[18]
c_{liq} (J/mole)	204.26	[18]
ρ (g/cm^3)	35.970	[18]
D (cm^2/s)	0.7×10^{-3}	[18]
d_0 (cm)	3.91×10^{-7}	[18]
k	0.06	b
d_0^c (cm)	2.0×10^{-6}	b
D^c (cm^2/s)	9.1×10^{-7}	b

[a]Sigma Chemical Co.
[b]This work.

The capillary length d_0^c calculated from these values is $d_0^c = 2.0 \pm 0.2 \times 10^{-6}$ cm. The diffusion length for a typical velocity of 2.9 μm/s is $l^c = 6.2 \times 10^{-3}$ cm. Values for the corresponding thermal parameters are $d_0 = 3.19 \times 10^{-7}$ cm and l=4.8 cm. The values of the various material parameters discussed in this section are summarized in Table I.

B. The selection parameter σ

The dimensionless parameter σ defined in Eq. (3.2) first arose in the linear stability analysis of dendrites by Langer and Muller-Krumbhaar which indicated that for free growth in three dimensions σ should have a constant value of $\sigma^* \sim 0.02$. With the subsequent development of microscopic solvability theory, it was shown that the selection parameter σ^* (the unique value of σ for which an allowed stable solution of the equations governing dendritic growth occurs) is indeed a material constant, but it depends on several specific material parameters, particularly the anisotropy of the crystal-melt interfacial tension [1]. For PVA, the anisotropy was recently determined to be (2.6±0.2)% and was found to be unaffected by addition of ethanol as an impurity up to 1%. The corresponding theoretical value for $\sigma*$ was 0.107±0.007. (For more details concerning this result and a recent comparison of experimental and theoretical σ values for various materials, see Ref. [19].)

In our dendritic sidebranching experiments, σ was treated as an adjustable fitting parameter for the sidebranching response curve [Eq. (3.3)] and for the growth of sidebranches [Eqs. (3.1) and (3.3)]. This gave values of σ between 0.057 and 0.078 for the response curve and between 0.037 and 0.051 for the growth of the sidebranches, as indicated in Table II. Using the values of d_0^c and D^c determined above, we can calculate the value of σ^c appropriate for dendritic growth from our binary mixture, and compare it to the values of σ extracted from the fits. Thus, defining

TABLE II. Values of σ.

Method of evaluation	Value
Sidebranch response curve [fits to Eq. (3.3)]	0.057–0.078
Sidebranch amplitude [fits to Eqs. (3.1) and (3.3)]	0.037–0.051
Direct determination from Eq. (5.3)[a]	0.008 ± 0.001
Value estimated from initial instability of planar interface	0.04 ± 0.02
Theoretical prediction based on measured anisotropy[b]	0.107 ± 0.007

[a]Value calculated for $v = 2.9$ μm/s and $\rho = 13.7$ μm.
[b]From Ref. [19].

$$\sigma^c = 2d_0^c D^c/\rho^2 v \tag{5.3}$$

and inserting the appropriate values, we find $\sigma^c = 0.008 \pm 0.001$. This value is approximately 8 times smaller than the values of σ obtained from the fits to Eq. (3.3). If σ had been fixed at this smaller value, the peak of $W(\bar{\tau})$ would occur at $\bar{\tau}_p = 1.5$, far below the experimental maximum at $\bar{\tau}_p \sim 4$. In the experiment of Bouissou *et al.* [10] with modulated flow of PVA-ethanol solution, the sidebranching response was a maximum for $\bar{\tau}_p \sim 7$, corresponding to $\sigma \sim 0.11$, while the theoretical response function peaks at ~ 4, corresponding to $\sigma \sim 0.04$. This discrepancy is qualitatively similar to what we have observed.

We further note that this value of $\sigma^c = 0.008$ is smaller than that measured in most other experiments [19], which led us to look for an independent way to determine σ^c. Since D^c was measured directly, the most likely problem in calculating σ^c comes from the determination of the capillary length d_0^c, which depends on all the parameters in Eq. (5.1). We have therefore made a preliminary attempt to estimate d_0^c independently by measuring the wavelength of the initial Mullins-Sekerka [20] instability of a planar interface. Wollkind and Segel [21] analyzed the initial instability of a planar interface in a temperature gradient. Their calculation, which employed a one-sided model, predicts the initial wavelength of the instability to be given by $\lambda_c = (4\pi D^c/v)(v d_0^c/4kD^c)^{1/3}$. Using this prediction to evaluate the capillary length, and in turn σ^c, gave $\sigma^c = 0.04 \pm 0.02$. Note that this determination of d_0^c is independent of the parameters in Eq. (5.1) except for k. These measurement are of a preliminary nature and are complicated by the flatness of the neutral stability curve predicted by linear stability theory (for a discussion of the problems associated with this measurement see Ref. [22]). This last value of σ^c does, however, overlap the range of values obtained by the fits to Eqs. (3.1) and (3.3). The values of σ found in our experiments are summarized in Table II.

VI. DISCUSSION AND CONCLUSIONS

We have shown that a localized thermal perturbation applied to the tip of a growing dendrite can dramatically alter the sidebranch structure, creating an ordered region of sidebranches of well-defined wavelength synchronous with the perturbation. The sidebranching response curve of the dendrite is qualitatively similar to the envelope of the spectrum of spontaneous sidebranches of the unperturbed dendrite. These observations are consistent with a model in which sidebranches arise as a result of the amplification of noise at the tip, and are then advected along the sides of the dendrite.

The theoretical sidebranching response function [Eq. (3.3) with $B(x) = x^2/2$] proposed by Barber, Barbieri, and Langer for the case of free growth is qualitatively similar to the response curve we have obtained for directional solidification of a binary mixture. The value of σ extracted from the fit is similar to the selected value of σ for several other systems [19]. However, the variation of σ with x, and the variation of σ with v does not seem consistent with the concept of σ as a material constant, as implied by microscopic solvability theory. Also, the value of σ found from the fits does not agree with the value of σ^c obtained by using Eq. (5.3) with the values of ρ and v obtained in this experiment.

From the fits of sidebranch amplitude to Eqs. (3.1) and (3.3), we find reasonable agreement with the prediction of Barber, Barbieri, and Langer for both the full function and the asymptotic approximation. However, the values of σ extracted from these fits is again higher than the value of σ^c calculated from Eq. (5.3). In comparing our data with Eqs. (3.1) and (3.3), one must appreciate that their derivations include linearizing the equations of motion for small perturbations around the steady state. Thus, since our data were taken far from the dendrite tip, the sidebranches have grown large enough to be well out of the linear regime in which these equations are strictly valid.

We note that the quantitative disagreement in σ values and the disagreement concerning the dependence of the response function on distance down the dendrite may both result from the neglect of nonlinearities. A more complete theory which takes account of nonlinear effects might resolve both of these disagreements.

Other possible sources of error include size effects due to performing the experiments in capillaries. Our capillaries have a width of 1000 μm and the chemical diffusion length is about 60 μm. Thus the tip is many diffusion lengths away from the capillary wall. However, further down the dendrite size effects could play a significant role in limiting the growth of the sidebranches. Another source of uncertainty is the possible dependence on the distance of the laser spot from the dendrite tip, which has not yet been explored. We note, however, that our results are qualitatively similar to those of Bouissou

et al. [10], who employed a global—rather than local—perturbation. A further possible source of problems is associated with applying a theory for free growth to directional solidification of a binary alloy. Although the selection parameter σ has been found to be reasonably independent of undercooling in free-growth experiments, there is no evidence that σ will be constant in directional solidification when the temperature gradient or growth speed is varied. In fact, a recent study by Trivedi and Mason [23] of directional solidification of PVA-ethanol indicates that $\sigma*$ determined from the dendrite tip radius changes systematically with composition and temperature gradient. Further work on the tip selection problem and the initial planar instability problem in crystal-dye systems during directional solidification is underway and will be presented in a later paper.

Note added. We have learned that in a recent (unpublished) experiment, A. V. Gorbunov (Chernogolovka) applied cw laser radiation to alkali halide crystals which produced "dendritic melting." Periodic modulation of the laser intensity was found to cause sidebranch ordering resembling the effects reported in this paper.

ACKNOWLEDGMENTS

We wish to thank O. Martin, M. N. Barber, J. S. Langer, P. Tabeling, and M. Ben Amar for helpful discussions and suggestions. We are particularly indebted to N. Goldenfeld for suggesting this experiment to us. This research was supported by the U.S. Department of Energy under Grant No. DE-FG02-84ER45132.

* Present address: IBM, Mail Stop E31-028, 5600 Cottle Rd., San Jose, CA 95139.

[1] J.S. Langer, in *Chance and Matter*, 1986 Les Houches Lectures, edited by J. Souletie, J. Vannimenus, and R. Stora (North-Holland, Amsterdam, 1987).
[2] D.A. Kessler, J. Koplik, and H. Levine, Adv. Phys. **37**, 255 (1988).
[3] E.A. Brener and V.I. Mel'nikov, Adv. Phys. **40**, 53 (1991).
[4] J.S. Langer, Phys. Today **45** (10), 24 (1992).
[5] R. Pieters and J.S. Langer, Phys. Rev. Lett. **56**, 1948 (1986); R. Pieters, Phys. Rev. A **37**, 3126 (1988).
[6] M.N. Barber, A. Barbieri, and J.S. Langer, Phys. Rev. A **36**, 3340 (1987).
[7] A. Dougherty, P.D. Kaplan, and J.P. Gollub, Phys. Rev. Lett. **58**, 1652 (1987).
[8] A. Dougherty and J.P. Gollub, Phys. Rev. A **38**, 3043 (1988).
[9] X.W. Qian and H.Z. Cummins, Phys. Rev. Lett. **64**, 3038 (1990).
[10] PH. Bouissou, A. Chiffaudel, B. Perrin, and P. Tabeling, Europhys. Lett. **13**, 89 (1990).
[11] M. Rabaud, Y. Couder, and N. Gerard, Phys. Rev. A **37**, 935 (1988).
[12] J.S. Langer, Physica A **140**, 44 (1986).
[13] Ya.B. Zel'dovich, A.G. Istratov, N.I. Kidin, and V.B. Librovich, Combust. Sci. Technol. **24**, 1 (1980).
[14] J.S. Langer, Phys. Rev. A **36**, 3350 (1987).
[15] D.A. Kessler and H. Levine, Europhys. Lett. **4**, 215 (1987).
[16] H. Chou and H.Z. Cummins, Phys. Rev. Lett. **61**, 173 (1988).
[17] J.S. Langer, Rev. Mod. Phys. **52**, 1 (1980).
[18] E.R. Rubenstein and M.E. Glicksman, J. Cryst. Growth **112**, 84 (1991).
[19] M. Muschol, D. Lui, and H.Z. Cummins, Phys. Rev. A **46**, 1038 (1992).
[20] W.W. Mullins and R.F. Sekerka, J. Appl. Phys. **35**, 444 (1964).
[21] D.J. Wollkind and L.A. Segel, Philos. Trans. R. Soc. **268**, 351 (1970).
[22] J.T.C. Lee, K. Tsiveriotis, and R.A. Brown, J. Cryst. Growth **121**, 536 (1992).
[23] R. Trivedi and J.T. Mason, Metall. Trans. A **22**, 235 (1991).

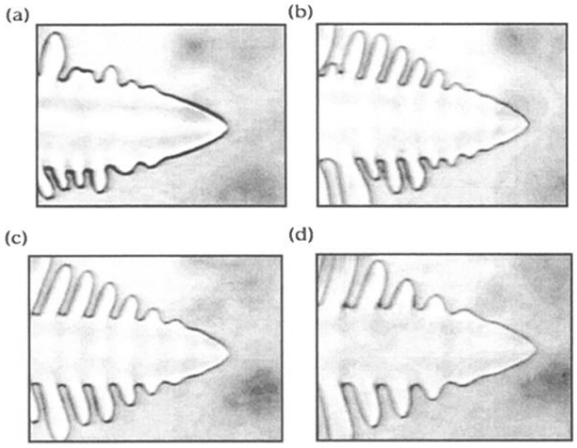

FIG. 2. Video images of dendrites grown by directional solidification from a mixture of pivalic acid and 0.44 wt. % coumarin 152. v=3.7 μm/s. (a) No perturbation; (b) 1-s laser pulses with a repetition rate of $\tau_r = 15$ s; (c) repetition rate of $\tau_r = 19$ s, which is close to the natural period; (d) repetition rate of $\tau_r = 26$ s.